Fabrication of Lotus-Type Porous Al-Si Alloys Using the Continuous Casting Technique

J.S. PARK, S.K. HYUN, S. SUZUKI, and H. NAKAJIMA

Lotus-type porous Al-Si (4, 8, 12, 14, and 18 wt pct) alloys were fabricated using the continuous casting technique under a hydrogen gas pressure of 0.1 MPa at various transference velocities, and the effects of the silicon content level and transference velocity on the pore morphology and porosity were investigated. Both the porosity and the average pore diameter increase as the silicon content level increases and decrease as the transference velocity increases. In particular, the velocity dependence is obviously exhibited at a silicon content level higher than 12 wt pct. The pore shape is changed from irregular in the higher-dendrite fraction to nearly circular in the lower-dendrite fraction. The porosity and the pore morphology are influenced by the silicon content level and transference velocity. In the model, these results can be understood with the explanation that the pores, which contribute to the increase in porosity, are generated at the eutectic fronts. This indicated that the porosity and the pore size in lotus-type porous Al-Si alloys can be well controlled by varying the silicon content level and the transference velocity.

I. INTRODUCTION

POROUS metals have unique characteristics that are different from those of bulk metals, such as an inherently low density and a large surface area. Thus, these metals are expected to be utilized as lightweight materials, catalysts, electrodes, vibration- and acoustic-energy-damping materials, impact-energy-absorbing materials, *etc.*[1,2] In particular, porous Al alloys are expected to be used for lightweight structural applications because of their low specific weight, high stiffness, and high energy-absorbing capacity.

Recently, lotus-type porous metals, one class of the porous metals, have been investigated by many researchers;[3–9] these materials possess long cylindrical gas pores aligned in one direction. Lotus-type porous metals have superior mechanical properties originating from unidirectional pores, compared with conventional porous metals, the pores of which are almost isotropic and spherical.[10] As a result, lotus-type metals are attracting attention as new lightweight structural materials.

Lotus-type porous metals have been developed based on the unidirectional solidification method, using the gas solubility gap between the liquid and the solid.[4–9,11] Recently, our group successfully fabricated a long-sized lotus-type porous copper slab using the continuous casting technique,[9,12,13] and we reported that both the porosity and pore size can be easily controlled by the solidification velocity and the hydrogen pressure in the continuous casting technique.

Lotus-type porous aluminum is also expected to be utilized as a lightweight structural material. For aluminum and its alloys, hydrogen is available for pore formation and growth.[9] However, it is difficult to obtain high porosity due to the small hydrogen gas solubility gap between the liquid and the solid.[14] Furthermore, in the case of casting in nonporous aluminum and its alloy, it is also reported that both the porosity and pore diameter are reduced at a high solidification rate, because there is no time for the hydrogen to diffuse from the aluminum into the pores.[14–16] Therefore, both an increase in the hydrogen gas solubility gap and control of the solidification rate are required in order to increase the porosity of the material.

It is thought that the addition of an alloying element is an effective method of changing pore formation. Silicon is one of the important alloying elements in Al alloys, and Al-Si alloys have been used as commercial cast alloys in various industrial fields. Pore formation in Al-Si alloys has been investigated by many researchers,[16–22] who reported that pores in cast-Al alloys are both shrinkage pores and gas pores caused by the rejected hydrogen from the solid to the liquid during solidification. However, these results largely bring pores into focus as the casting defect of Al-Si alloys. The effect of a silicon addition to lotus-type porous Al-Si alloys has not yet been studied.

In this study, lotus-type porous Al-Si alloys containing various silicon content levels were fabricated by the continuous casting technique at various transference velocities and under a hydrogen gas pressure of 0.1 MPa. The effects of the silicon content level and the transference velocity on the porosity, pore size, and pore morphology were then investigated.

J.S. PARK, Specially Appointed Assistant Professor, S. SUZUKI, Associate Professor, and H. NAKAJIMA, Professor, are with The Institute of Scientific and Industrial Research, Osaka University, Osaka 567-0047, Japan. Contact e-mail: park23@sanken.osaka-u.ac.jp S.K. HYUN, formerly Associate Professor, The Institute of Scientific and Industrial Research, Osaka University, is Assistant Professor with the School of Materials Science and Engineering, Inha University, Inchon 402-751, South Korea.

II. EXPERIMENTAL PROCEDURES

The continuous casting apparatus used in this study is shown in Figure 1. In a crucible, a suitable amount of both pure aluminum ingots (99.99 wt pct Al) and Al-35 wt pct Si ingots were prepared to obtain Al-Si with the nominal Si content level of 4, 8, 12, 14, and wt pct Si. The ingots in the crucible were melted together by radio-frequency induction heating under a hydrogen gas pressure of 0.1 MPa in the chamber. After the temperature reached 1173 K, the melt was maintained for 600 seconds, in order to sufficiently dissolve and diffuse the hydrogen in the melt. Subsequently, the melt was pulled down by a dummy bar of nonporous pure aluminum through a cooled mold (10 mm in thickness and 30 mm in width) at a given velocity. The transference velocity was set to various values, such as 1, 1.5, 2, and 5 mm min^{-1}, in order to investigate the effect of solidification velocity on the porosity, pore size, and pore morphology. The transference velocity was mechanically controlled by the rotational speed of the pinch rollers.

The fabricated lotus-type slabs were cut using a spark-erosion wire-cutting machine, model LN1W (Sodick Co. Ltd., Yokohama, Japan), in directions both parallel and perpendicular to the transference direction (TD). Each cross section was polished with a series of emery papers and etched by a 10 pct NaOH solution for 300 seconds. The microstructures were then observed using an optical microscope. The pore diameter and circularity and the area fraction of the primary α phase were measured on the cross section perpendicular to the TD by a WinROOF image analyzer (Mitani Corporation, Tokyo, Japan). The effective pore diameter was the diameter of a circle that has the same area as the pore. The pore circularity was calculated by Eq. [1]. If the value of the pore circularity evaluated by the following equation approaches 1.0, the pore shape becomes the circle:

$$\text{pore circularity} = 4\pi \times \frac{\text{area of a pore}}{(\text{the circumference of a pore})^2}$$
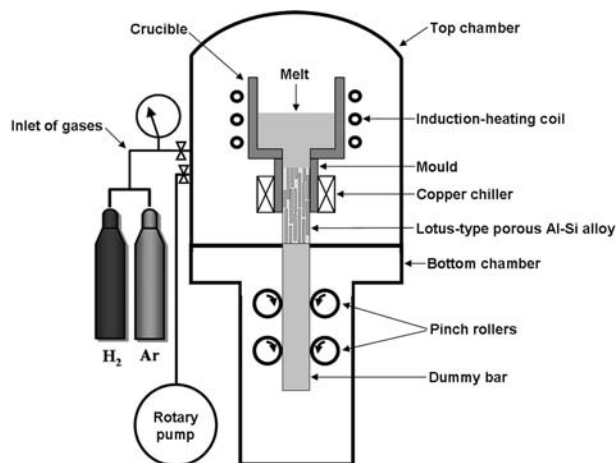
[1]

Fig. 1—Schematic drawings of the continuous casting apparatus.

The average value and standard deviation in both the pore diameter and pore circularity were obtained from the results measured above 30 pores in each condition. The area fraction of the primary α-Al phase was measured within an area that does not include pores.

The porosity (p) was evaluated from the following expression:

$$p\,(\text{pct}) = \left(1 - \frac{\text{apparent density of porous Al} - \text{Si alloy}}{\text{density of nonporous Al} - \text{Si alloy}}\right) \times 100$$

[2]

The apparent density of the individual specimen was calculated by measuring both the weight and the apparent volume of each fabricated slab.

III. RESULTS

Figure 2 shows the cross-sectional views parallel and perpendicular to the TD of the slabs fabricated by the continuous casting technique at various transference velocities. The porosity and pore morphology are changed by both the silicon content level and the transference velocity.

The porosity measured in each fabricated slab increases with an increase in the silicon content level at all velocities and increases with a decrease in the velocity, as exhibited in Figure 3. The velocity dependence of the porosity becomes more significant at a silicon content level higher than 12 wt pct.

Figure 4(a) shows the effect of the silicon content level and transference velocity on the average pore diameter; this was evaluated using the cross-sectional views in Figure 2. It is unusual that the pore diameter has a bimodal distribution at 1.0 mm min^{-1} at silicon content levels of 12, 14, and 18 wt pct. This type of bimodal distribution may be attributed to the combination and coarsening of plural single pores; other bimodal distributions are due simply to the growth of individual pores. Thus, the mechanism of pore formation is different. The histograms of the pore diameter were fitted to the Gaussian function by weighting them according to the frequency of the pores. Because the number of small pores is much larger than the number of large pores, the average pore diameter obtained by the fitting was estimated as the value closest to the size of the small pores. In order to avoid such evaluations, the average pore diameter of the large-pore group was separately obtained by fitting it to the Gaussian function without the small-pore group. Figure 4(b) exhibits the average pore diameters in each group of small and large pores; a similar bimodal distribution was also observed in the lotus-type porous copper fabricated at 1.0 mm min^{-1} using the continuous casting technique.[13]

In Figure 4(a), the average pore diameter changes with the silicon content level. In the range between 4 and 8 wt pct Si, the average pore diameter does not vary significantly and is independent of both the silicon content level and the transference velocity. At silicon
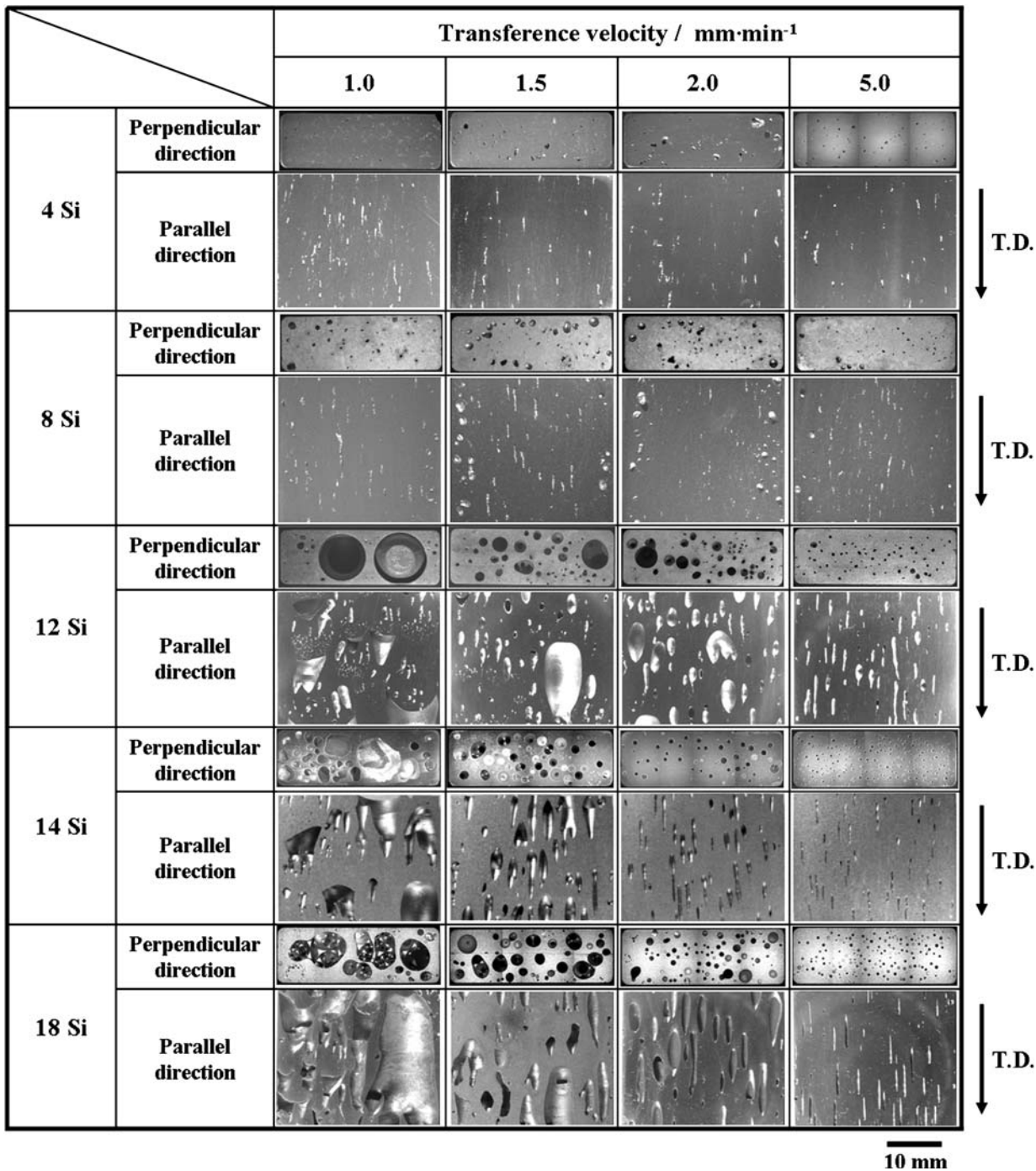
Fig. 2—Cross sections perpendicular and parallel to the TD of lotus-type porous Al-*x* wt pct Si (*x* = 4, 8, 12, 14, and 18) alloys fabricated at various transference velocities under a hydrogen gas pressure of 0.1 MPa. Arrows show TD.

content levels over 8 wt pct, the average pore diameter increases as the silicon content level increases. In this range, the average pore diameter increases primarily as the transference velocity decreases.

The bimodal distribution occurs in the case in which large pores are generated by the cohesion of a few small pores at a low transference velocity.[7,8] Because the inhomogeneous pore formation and growth occurs in the whole slab, the pore distribution changes in the

longitudinal direction. Therefore, the result of the bimodal distribution is not included in the following discussion.

Figure 5 shows the effect of the silicon content level on pore circularity investigated at 2.0 mm min⁻¹. This velocity was selected because the pore distribution is relatively homogeneous across the entire range of the concentration. Pore circularity increases as the silicon content level increases. This means that the shape of the
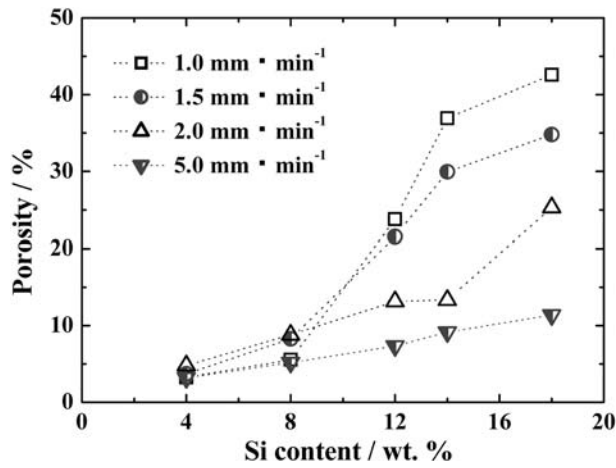
Fig. 3—Porosity *vs* silicon content level of lotus-type porous Al-Si alloys fabricated at various transference velocities under a hydrogen gas pressure of 0.1 MPa.
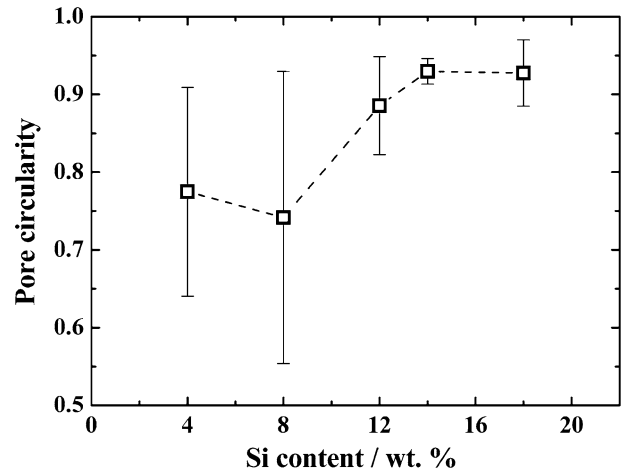

Fig. 5—Pore circularity *vs* silicon content level of lotus-type porous Al-Si alloys fabricated a at a transference velocity of 2.0 mm min^{-1} under a hydrogen gas pressure of 0.1 MPa. Error bars are standard deviations.
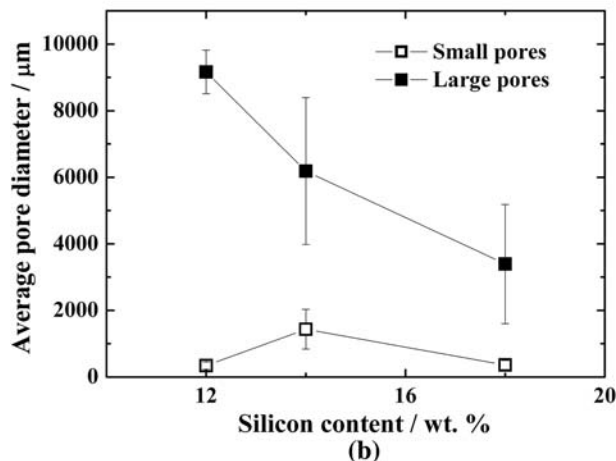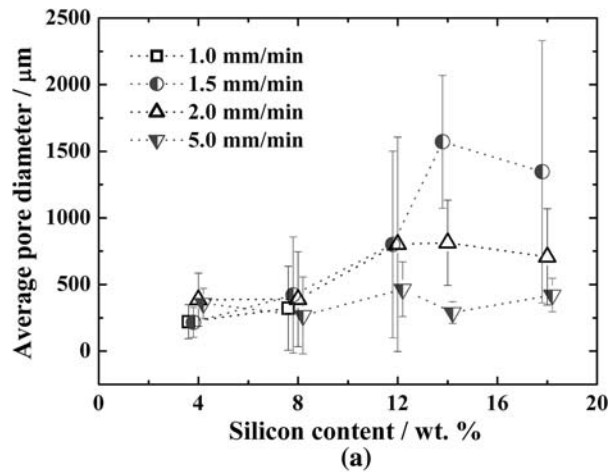

Fig. 4—(*a*) Silicon-content dependence of the average pore diameter of lotus-type porous Al-Si alloys fabricated at various transference velocities under a hydrogen gas pressure of 0.1 MPa. (*b*) Silicon-content dependence of the average pore diameter in each group of small and large pores. A bimodal distribution was observed in the range of Si content levels from 12 to 18 wt pct at a transference velocity of 1 mm min^{-1}. Error bars are standard deviations.

pores is irregular when the silicon content level is between 4 and 8 wt pct; it is nearly circular when the silicon content level is over 12 wt pct.

With changing silicon content levels, the microstructures are also changed, as shown in Figure 6. Figures 6(a) through (e) show the microstructures perpendicular to the TD at various silicon content levels, at a velocity of 2.0 mm min^{-1}. Figure 6(f) shows the magnified microstructure of the dashed square region in Figure 6(e). In Figures 6(a) through (e), the white region corresponds to the primary α-Al, and the area fraction of the primary α-Al decreases as the silicon content level increases, as exhibited in Figure 7. In particular, neither the primary α-Al nor the primary Si can be observed in Figures 6(e) and (f). Hence, it is thought that the eutectic composition of Si is located at approximately 18 wt pct in Al-Si alloys fabricated at 2.0 mm min^{-1} in this study. On the other hand, primary Si is observed in the slabs fabricated at 1.0 and 1.5 mm min^{-1}.

The change in the microstructure and the pores caused by the transference velocity is displayed in Figure 8, which shows the microstructures both perpendicular and parallel to the TD of Al-12 wt pct Si alloys fabricated at various transference velocities. Both the dendritic primary α-Al and the pores are approximately aligned in one direction parallel to the TD, and the pores are located in the channels that exist among the columnar dendrites. In addition, both the pore volume and the growth direction are affected by the density of the dendritic primary α-Al.

IV. DISCUSSION

It is reported that the porosity in lotus-type porous pure metals depends on the amount of hydrogen rejected from the solid during unidirectional solidification; this is related to the hydrogen gas solubility gap between the liquid and the solid.[4,6,13] The hydrogen gas
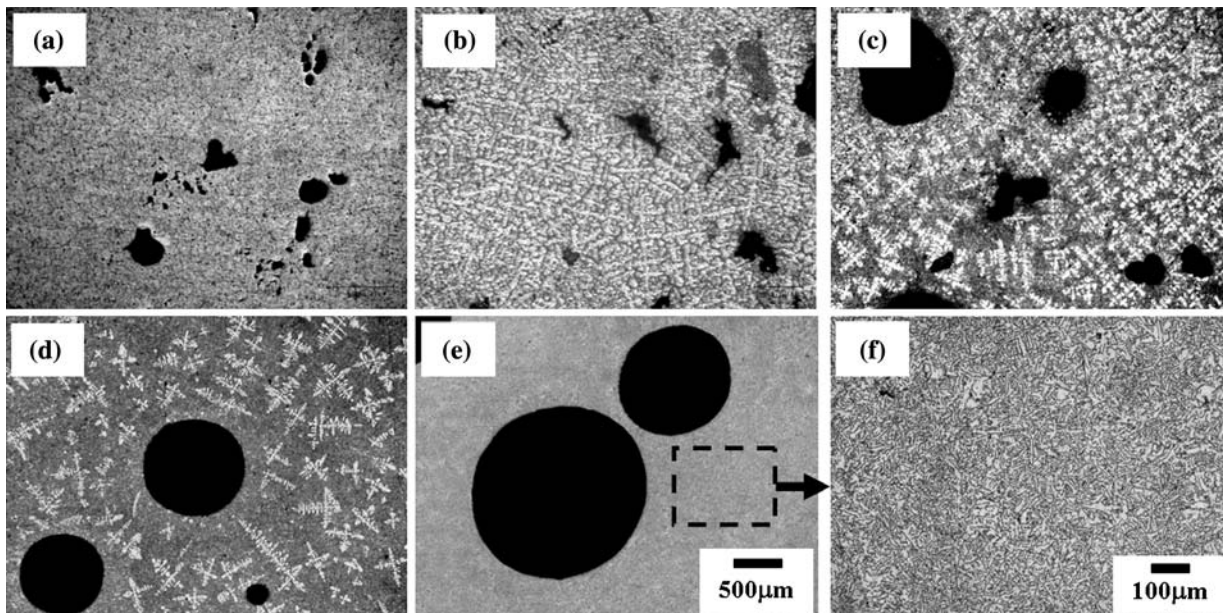
Fig. 6—Microstructures perpendicular to TD at each silicon content level of Al-Si alloys fabricated at a velocity of 2.0 mm min^{-1} under a hydrogen gas pressure of 0.1 MPa: (*a*) 4, (*b*) 8, (*c*) 12, (*d*) 14, and (*e*) 18 wt pct Si. (*f*) Partly magnified image of (e). (a) through (e) are shown at the same magnification.
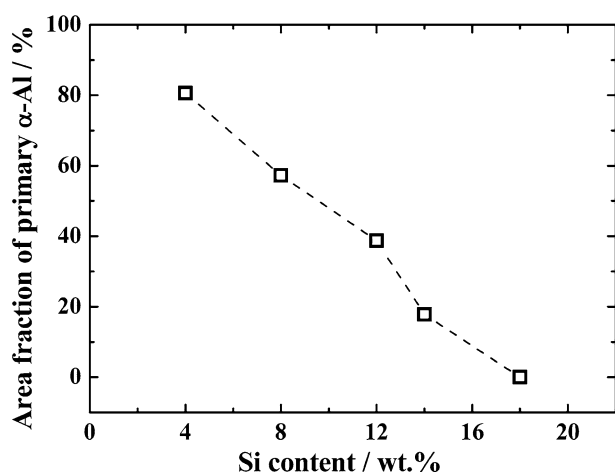

Fig. 7—Area fraction of primary α-Al *vs* silicon content level of lotus-type porous Al-Si alloys fabricated at a transference velocity of 2.0 mm min^{-1} under a hydrogen gas pressure of 0.1 MPa.

solubility in the liquid and the solid phase is proportional to the root of the partial pressure of hydrogen, according to Sieverts' law, at the melting temperature in a metal-hydrogen system.[4–6,13] Therefore, we started the discussion with the assumption that the porosity in Al-Si alloys also depends on the amount of hydrogen rejected from the solid during solidification.

Although hydrogen solubility in aluminum and its alloys has been investigated by many researchers,[14,15,18,22,23] the data related to hydrogen solubility in Al-Si alloys are limited. It was reported that liquid pure silicon has a higher hydrogen solubility than liquid pure aluminum at a given temperature and under a given pressure.[24] However, Opie and Grant[14] reported that the hydrogen solubility of the liquid Al-Si alloy is

lower than that in both pure aluminum and pure silicon. Hence, the hydrogen solubility in liquid Al-Si alloys cannot be estimated by interpolating between pure Al and pure Si. The cause of the decrease in hydrogen solubility with the Si addition is explained as the change in the hydrogen behavior in aluminum that occurs because of alloying.

In order to evaluate the hydrogen solubility using the silicon content levels in this study, we attempted to calculate the amount of the hydrogen solubility gap at the melting point. To calculate the hydrogen solubility in the liquid, the equation for the hydrogen solubility of pure aluminum and some Al-Si alloys in the liquid was used; this was suggested by Opie and Grant.[14] The hydrogen solubility S of liquid pure aluminum and liquid Al-Si alloys is calculated using the following empirical equation:[14]

$$\log_{10} S = -\frac{A}{T} + B \qquad [3]$$

where T is the temperature and A and B are constants that depend on the Si content, as shown in Table I. The hydrogen solubilities of Al-Si alloys with 12, 14, and 18 wt pct Si are evaluated by interpolating and extrapolating the results calculated using Eq. [3].

The temperature is evaluated from the liquidus line of each composition in the Al-Si equilibrium phase diagram.[25]

For the solid, the solubility data available from pure aluminum[14] were used instead of those from Al-Si alloys, with the assumption that the hydrogen solubility of the solid Al-Si alloy is not significantly different from that of pure aluminum. The hydrogen solubility of solid pure aluminum was assumed to have a linear relationship with the temperature; this goes through the
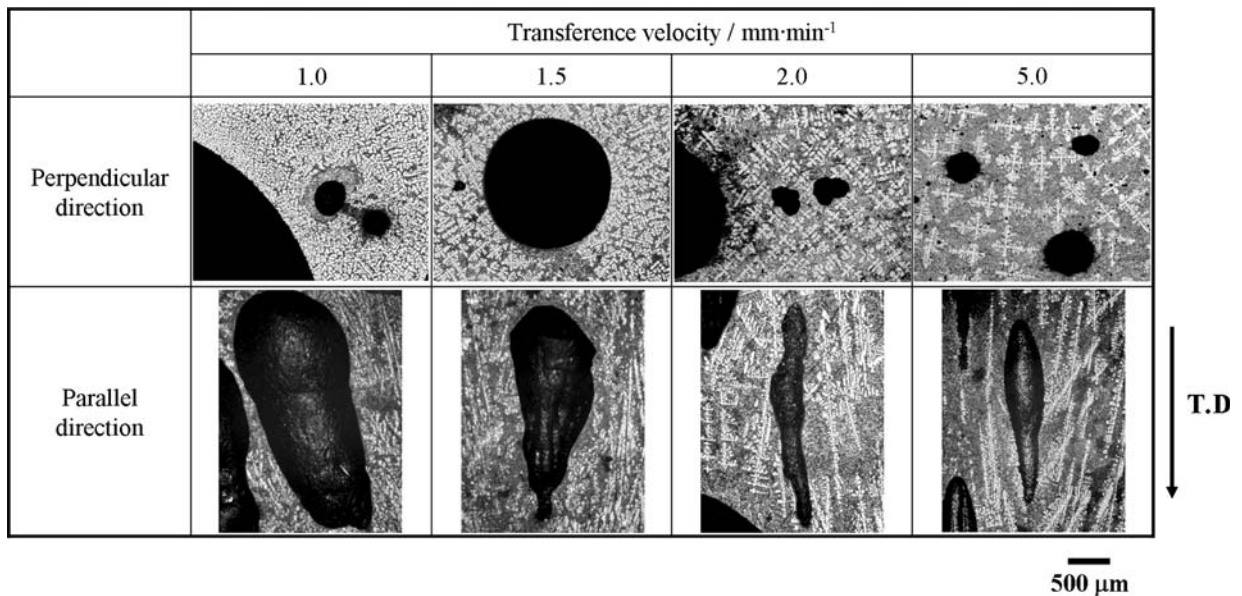
Fig. 8—Microstructures and pores perpendicular and parallel to the TD of lotus-type porous Al-12 wt pct Si alloys fabricated at various transference velocities under a hydrogen gas pressure of 0.1 MPa. Arrow shows TD.

Table I.   Values of Constants *A* and *B* in Eq. [3] in the Liquid of Pure Aluminum and Al-Si Alloys

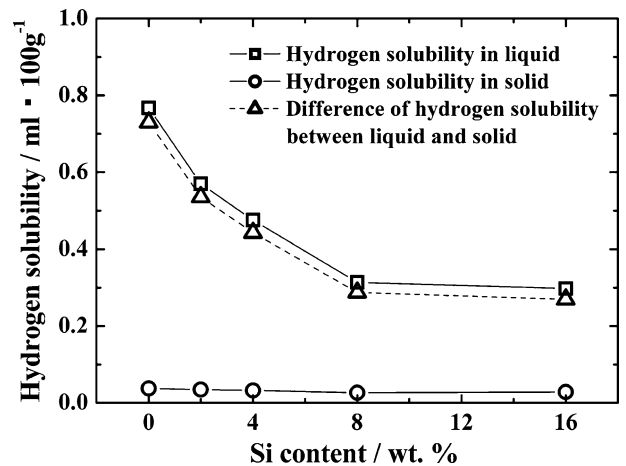| Composition	*A*	*B*
Pure aluminum	2550	2.62
Al-2 wt pct Si	2800	2.79
Al-4 wt pct Si	2950	2.91
Al-8 wt pct Si	3050	2.95
Al-16 wt pct Si	3150	3.00

Fig. 9—Hydrogen solubility of the liquid and solid of pure Al and some Al-Si alloys and the difference in the amount of hydrogen in the liquid and solid. Hydrogen solubility of the liquid is evaluated by the equation reported by Opie and Grant.[14] For the hydrogen solubility of the solid, the value of the hydrogen solubility in pure Al is used.

reference data of 0.04 cc·100 g Al^{-1} (at 933 K) and 0.036 cc·100 g Al^{-1} (at 873 K).[14]

Figure 9 shows the calculated hydrogen solubility in each composition. The hydrogen solubility in liquid Al-Si alloys drastically decreases as the silicon content level increases. The hydrogen gas solubility between the liquid and the solid, which should correspond to the amount of rejected hydrogen during solidification, also decreases as the silicon content level increases. However, the calculated results do not agree with the experimental results, which show that the porosity increases as the silicon content level increases, as shown in Figure 3.

As shown in the velocity condition of 2 mm min^{-1} in Figure 2, it seems that pore formation and growth were generally promoted more through an increase in the silicon content level, although the amount of absolute hydrogen rejected from the solid decreases as the silicon content level increases, as shown in Figure 9. This means that the pores form and grow easily, even though the amount of hydrogen rejected from the solid during solidification decreases as the silicon content level increases. Hence, it is thought that the increase in porosity that occurs as the silicon content level increases is caused by the increase in the gas pores grown unidirectionally during solidification; it is also thought that pore formation and growth in the lotus-type porous

Al-Si alloys are closely related to the complicated solidification mode of Al-Si alloys, which is different from that of pure metals such as copper. Thus, in order to clarify the reason for the increase in porosity as the silicon content level increases, the pore formation and growth mechanism was investigated in the lotus-type porous Al-Si alloys during solidification. In the lotus-type porous metals, it is well known that pore formation and growth occur at the solid-liquid interface, so that the porosity depends only on the amount of hydrogen rejected from the solid during solidification, which is related to the hydrogen gas solubility gap between the liquid and the solid. However, the hypoeutectic Al-Si

alloy observed in this study has two kinds of solid-liquid interface; the liquid/primary α-Al and the eutectic front, as shown in Figure 10. Thus, it is thought that the porosity is affected by the hydrogen rejected from each interface of pore formation and growth.

Considering the solidification mode of Al-Si alloys, a model of the pore formation and growth that occur during the solidification process is suggested in this study, as shown in Figure 10. Hydrogen is rejected from both the primary α-Al and the eutectic front. However, for the following reasons, it is thought that the large pores, which contribute to the increase in porosity, are formed at the eutectic front but not at the liquid/primary α-Al interface; the pores then grow in the channels among the columnar dendrites along the solidification direction, with the movement of the eutectic front.

First, as shown in Figure 8, the pores are located in the channels among the columnar dendrites and are directed along the columnar dendrites.

Second, the pore circularity is also related to this model. As shown in Figure 11, The pore growth is restricted within the channels among the columnar dendrites with the higher primary α-Al fraction.[16–20,26] Thus, the pore morphology becomes irregularly shaped, and the pore circularity increases as the eutectic fraction increases.
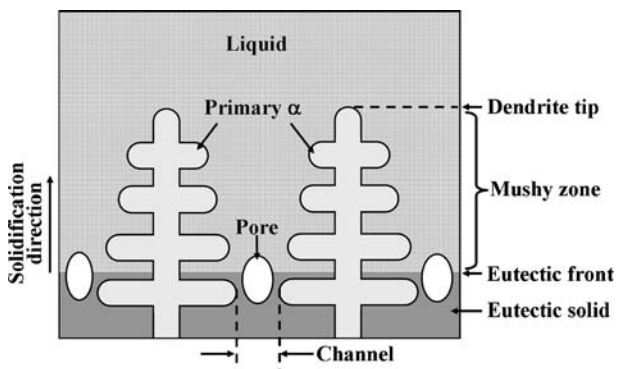
Third, following this model, the porosity should increase as the fraction of the eutectic phase increases. To confirm this assumption, we checked the relationship between the fraction of the eutectic phase and the amount of hydrogen rejected from the eutectic phase related to the porosity.

The eutectic composition is 12.6 wt pct Si in the equilibrium Al-Si binary-phase diagram.[25] However, the eutectic composition in this study is out of the equilibrium state, due to supercooling through the increase in the solidification velocity, and is near 18 wt pct Si at 2.0 mm min^{-1}, as shown in Figures 6 and 7. Assuming the eutectic composition under this condition is set up to 18 wt pct Si, the eutectic fraction in each silicon content level can be evaluated by the lever rule at the eutectic line of the nonequilibrium Al-Si binary-phase diagram.[25] The eutectic fraction calculated in the phase diagram is exhibited in Figure 12, along with that measured by the image analyzer.

The amount of rejected hydrogen is indicated by the upper line in Figure 13, which corresponds to the difference in the hydrogen solubility between the liquid
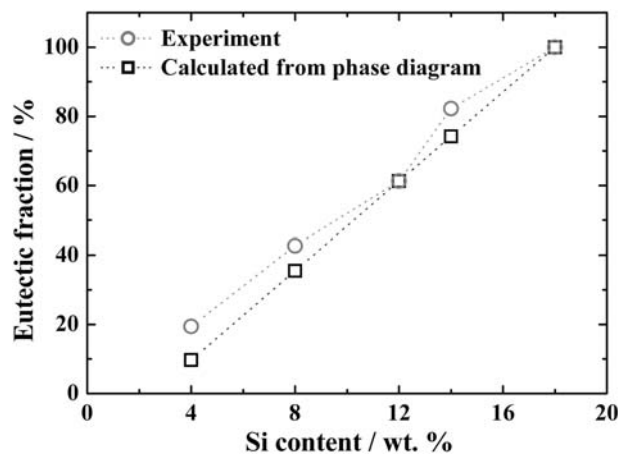

Fig. 10—Schematic drawing of the solid-liquid interfaces and pore formation during columnar dendritic solidification in hypoeutectic Al-Si alloy.

Fig. 12—Eutectic fraction vs silicon content level. ○: measured eutectic fraction by image analyzer on the cross section perpendicular to the TD of each Si content level for Al-Si alloy fabricated at 2.0 mm min^{-1} (as shown in Fig. 6). □: calculated from the Al-Si alloy metastable phase diagram in which the eutectic composition is 18 wt pct Si.[25]
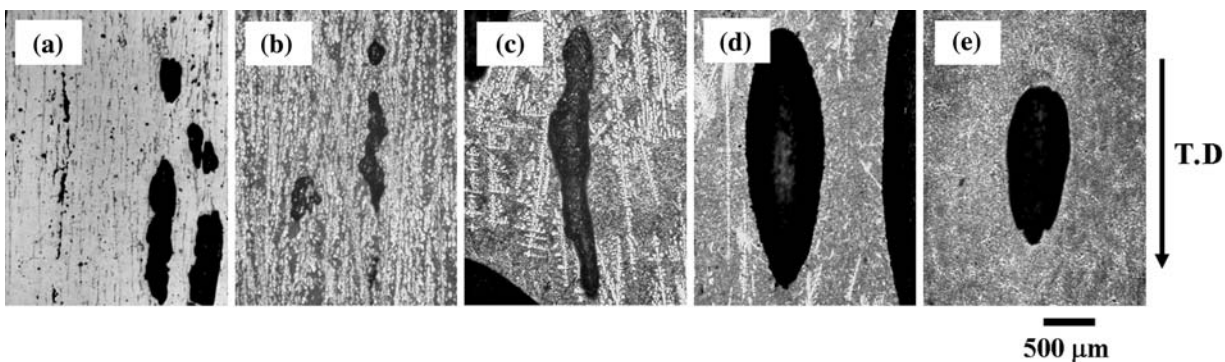

Fig. 11—Microstructures and pores parallel to TD at each silicon content level for Al-Si alloys fabricated at a velocity of 2.0 mm min^{-1} under a hydrogen gas pressure of 0.1 MPa: (a) 4, (b) 8, (c) 12, (d) 14, and (e) 18 wt pct Si.
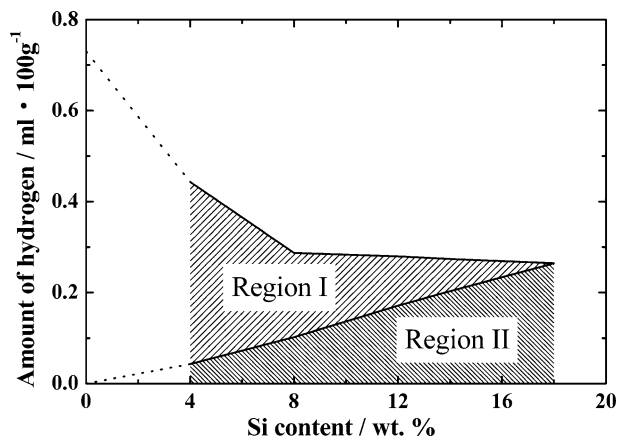
Fig. 13—Calculated values of the amount of hydrogen rejected from the solid during solidification; region I and region II represent the amount of hydrogen rejected from the primary α-Al and eutectic phase, respectively.

and solid, as shown by the triangle plots in Figure 9. Here, it is assumed that the amount of hydrogen rejected in a unit volume is constant for each phase of the primary α-Al and the eutectic phase and is in proportion to the area fraction of each phase. Hence, the rejected hydrogen in Figure 13 can be divided into two regions, according to the area fractions of the phases. Regions I and II represent the amount of hydrogen rejected from primary α-Al and the eutectic phase, respectively. The ratio between regions I and II corresponds to that of the area fractions of the phases shown in Figure 12. Although the values are only roughly estimated, it is considered that the tendency of the amount of hydrogen against the eutectic fraction can be predicted.

Although the total amount of hydrogen (region I + region II) decreases as the silicon content level increases, the amount of rejected hydrogen from the eutectic phase (region II) increases as the silicon content level increases. This result indicates that the amount of hydrogen for formation and growth of pores increases as the eutectic fraction increases. Thus, it is thought that both the porosity and the average pore diameter increase as the silicon content level increases.

The pore formation and growth mechanism can be explained from the point of view of hydrogen diffusion. If the pores formed near the solid-liquid interface grow as the interface is moved, as shown in Figure 10, it is considered that the hydrogen diffused into the pores is mainly related to that rejected from the eutectic solid. On the other hand, it is thought that the hydrogen rejected from primary α-Al during solidification diffuses via the mushy zone to the liquid, so that the hydrogen rarely affects the pore formation and growth. Even if the pores are formed by rejection of the hydrogen from the primary α-Al phases, the pores cannot grow large enough to contribute to the increase in porosity, due to the disturbance by the secondary dendrite arms.[16,17,20,26]

The hydrogen diffusion also corresponds to the decrease in both the porosity and pore diameter caused by the increase in the transference velocity at silicon content levels higher than 12 wt pct, as shown in Figures 3 and 4. This result is in good agreement with the decrease in both the porosity and the pore diameter caused by the increase in the solidification velocity in the pure aluminum and in the Al-Si and Al-Cu alloys that is reported by Sinada et al.[15] and Lee et al.,[16,17] respectively. These authors explained that most of the hydrogen has diffused into the pores at a low velocity, while the hydrogen does not have enough time to diffuse into the pores at a high velocity. Thus, it is thought that the pore diameter and porosity decrease as the transference velocity increases because of the decrease in the amount of hydrogen diffused in each pore during solidification.

The suggestion in this study that pore formation relates strongly to the eutectic phase corresponds to the reports about defects in the Al-Si alloy made by Dahle et al.[21] and Iwahori et al.[22] These authors reported that defects such as solidification shrinkage and hydrogen gas pores in Al-Si alloys are formed with the solidification of the eutectic phase.

V. CONCLUSIONS

The lotus-type porous Al-Si alloys were fabricated by the continuous casting technique under the hydrogen gas pressure of 0.1 MPa at various velocities; the maximum porosity of approximately 40 pct can be obtained at 1.0 mm min^{-1} in 18 wt pct Si.

Both the porosity and the average pore diameter increase as the silicon content level increases and decrease as the transference velocity increases. In particular, the velocity dependence is obviously exhibited at silicon content levels higher than 12 wt pct. The pore shape is changed from irregular in the higher-dendrite fraction to nearly circular in the lower-dendrite fraction. In this study, the porosity and pore morphology are governed by the silicon content level and the transference velocity.

The results of this study provide new information about pore formation in alloys, which is different from pore formation in pure metals. The discussion about pore formation in lotus-type porous Al-Si alloys requires consideration of both the complicated solidification mode and the hydrogen gas solubility gap between the liquid and the solid. The increase in porosity with the increasing silicon content level can be explained by the model that the pores that contribute to the increase in porosity are generated at the eutectic fronts.

The change in both the porosity and pore diameter by the transference velocity at silicon content levels higher than 12 wt pct is related to the hydrogen diffusion. Because the solidification time decreases as the transference velocity increases, the rejected hydrogen from the eutectic phase does not have enough time to diffuse into the pores at high velocity. Thus, it is thought that the amount of hydrogen diffused in each pore during solidification decreases as the transference velocity increases, so that the pore diameter and the porosity decrease as the transference velocity increases. Consequently, porosity and pore size in lotus-type porous Al-Si alloys can be well controlled through the silicon content level and the transference velocity.

Because Al-Si alloys are commonly used and representative eutectic systems, the results for Al-Si in this study are expected to provide information important to a discussion of the pore formation in other eutectic systems and solidification modes.

REFERENCES

1. A.G. Evans, J.W. Hutchinson, and M.F. Ashby: *Prog. Mater Sci..*, 1999, vol. 43, pp. 171–221.
2. J. Banhart: *Prog. Mater Sci..*, 2001, vol. 46, pp. 559–632.
3. V.I. Shapovalov: *Mater. Sci. Forum*, 1996, vols. 215–216, pp. 485–88.
4. S. Yamamura, H. Shiota, K. Murakami, and H. Nakajima: *Mater. Sci. Eng., A*, 2001, vol. 318, pp. 137–43.
5. S.K. Hyun and H. Nakajima: *Mater. Trans.*, 2002, vol. 43, pp. 526–31.
6. T. Nakahata and H. Nakajima: *Mater. Sci. Eng., A*, 2004, vol. 384, pp. 373–76.
7. S.K. Hyun and H. Nakajima: *Mater. Lett.*, 2003, vol. 57, pp. 3149–54.
8. T. Ikeda, T. Aoki, and H. Nakajima: *Metall. Mater. Trans. A*, 2005, vol. 36A, pp. 77–86.
9. H. Nakajima: *Prog. Mater. Sci.*, 2007, vol. 52, pp. 1091–1173.
10. S.K. Hyun, K. Murakami, and H. Nakajima: *Mater. Sci. Eng., A*, 2001, vol. 299, pp. 241–48.
11. H. Nakajima: *Mater. Trans.*, 2001, vol. 42, pp. 1827–29.
12. S.K. Hyun, J.S. Park, M. Tane, and H. Nakajima: in *Porous Metals and Metal Foaming Technology*, H. Nakajima and N. Kanetake, eds., Japan Institute of Metals, Sendai, Japan, 2006, pp. 211–14.
13. J.S. Park, S.K. Hyun, S. Suzuki, and H. Nakajima: *Acta Mater.*, 2007, vol. 55, pp. 5646–54.
14. W.R. Opie and N.J. Grant: *Trans. AIME*, 1950, vol. 188, pp. 1237–41.
15. Y. Shinada, Y. Ueda, and S. Nishi: *J. Jpn. Inst. Light Met.*, 1980, vol. 30, pp. 384–89.
16. R.C. Atwood, S. Sridhar, W. Zhang, and P.D. Lee: *Acta Mater.*, 2000, vol. 48, pp. 405–17.
17. P.D. Lee and J.D. Hunt: *Acta Mater.*, 2001, vol. 49, pp. 1383–98.
18. Y. Shinada, Y. Ueda, and S. Nishi: *J. Jpn. Inst. Light Met.*, 1983, vol. 33, pp. 508–17.
19. R.C. Atwood and P.D. Lee: *Metall. Mater. Trans. B*, 2002, vol. 33B, pp. 209–21.
20. A.M. Samuel and F.H. Samuel: *J. Mater. Sci.*, 1992, vol. 27, pp. 6533–63.
21. A.K. Dahle, J. Taylor, and D.A. Graham: *Alum. Trans.*, 2000, vol. 3, pp. 17–29.
22. H. Iwahori, K. Yonekura, Y. Yamamoto, and M. Nakamura: *AFS Trans.*, 1990, vol. 98, pp. 167–73.
23. M. Ichimura, Y. Sasajima, and M. Imabayashi: *Mater. Trans.*, 1992, vol. 33, pp. 449–53.
24. F.D. Manchester: *Phase Diagrams of Binary Hydrogen Alloys*, ASM INTERNATIONAL, Materials Park, OH, 2000, pp. 4 and 197.
25. J.L. Murray and A.J. McAlister: *Bull. Alloy Phase Diagrams*, 1984, vol. 5, pp. 74–84.
26. P.D. Lee and J.D. Hunt: *Acta Mater.*, 1997, vol. 45, pp. 4155–69.